Wood Sci Technol (2018) 52:209–227
https://doi.org/10.1007/s00226-017-0970-1

ORIGINAL

FTIR-based models for assessment of mass yield and biofuel properties of torrefied wood

Chi-Leung So[1] · **Thomas L. Eberhardt**[2]

Received: 19 September 2017 / Published online: 4 November 2017
© Springer-Verlag GmbH Germany (outside the USA) 2017

Abstract Biofuel properties can be improved through torrefaction, whereby the biomass is treated with moderately elevated temperatures (200–300 °C) under conditions that are essentially anaerobic and at atmospheric pressure. Varying the torrefaction conditions of temperature and treatment duration, as well as any feedstock pretreatments (drying, grinding), can generate products having varying degrees of thermal degradation, thus impacting performance in subsequent biofuel applications (e.g., gasification, pyrolysis, combustion). Pulp-grade pine wood chips were processed through a laboratory-scale crucible furnace retort with the remaining solid carbonized products subjected to ultimate, proximate, and spectroscopic analyses. Compared to air-dry wood chips, lower mass yields (i.e., greater thermal degradation) resulted from oven drying or grinding pretreatments. Regarding the torrefaction conditions, the degree of thermal degradation varied to a greater extent as a function of applied temperature than treatment duration. Furthermore, mass yield explained 95% of the variation in higher heating value. Fourier transform infrared (FTIR) spectroscopy combined with principal component analysis gave plots in which sample points clustered by torrefaction temperature and time, as well as by sample type (i.e., with or without pretreatment). Partial least squares regression was able to accurately predict mass yield and to a lesser extent carbon content. Results suggest that FTIR monitoring of finely ground samples in a production environment could be used off-line as a rapid assessment technique for mass yield and therefore facilitate adjustments to process parameters of temperature and/or treatment duration.

✉ Chi-Leung So
cso@agcenter.lsu.edu

[1] School of Renewable Natural Resources, Louisiana State University Agricultural Center, Baton Rouge, LA 70803, USA

[2] USDA Forest Service, Forest Products Laboratory, Madison, WI 53726, USA

Introduction

Torrefaction, a thermal process applied to biomass feedstocks that is essentially anaerobic, under atmospheric pressure, and within the temperature range of 200–300 °C (Chew and Doshi 2011; Ciolkosz and Wallace 2011; van der Stelt et al. 2011), has been used in biofuel applications for property enhancements including greater resistance to moisture uptake, reduced fungal degradation, higher carbon density, and increased grindability (Arias et al. 2008; Chen and Kuo 2011; Medic et al. 2012). Greater feedstock consistency following preprocessing by torrefaction can augment pyrolysis (Meng et al. 2012; Wannapeera et al. 2011), gasification (Couhert et al. 2009; Deng et al. 2009; Prins et al. 2006a), and combustion (Bridgeman et al. 2008) operations. However, torrefaction is not always beneficial for biofuel upgrading; during pelletization, torrefied wood affords greater friction in the pellet mill and lowers compression strength of the resultant pellets (Li et al. 2012; Na et al. 2013; Rudolfsson et al. 2015; Stelte et al. 2011).

Mass yields of solid material from the torrefaction of woody biomass feedstocks are reported to range between 70 and 90% (Ciolkosz and Wallace 2011). Losses in mass result from chemical changes to the cell wall polymers (hemicelluloses, cellulose, and lignin) as a function of both selected torrefaction temperature and treatment duration. The losses in mass among each of the cell wall polymers are not proportional, with a group of polysaccharide polymers, the hemicelluloses, being the most susceptible to thermal degradation. These polysaccharide polymers soften at temperatures below 200 °C and undergo a wide spectrum of modifications including deacetylation, dehydration, and depolymerization reactions between 200 and 300 °C (Couhert et al. 2009; Ciolkosz and Wallace 2011; Pushkin et al. 2015); among the hemicelluloses, the xylans are particularly susceptible to thermal degradation (Prins et al. 2006b, c; Werner et al. 2014). Below 250 °C, cellulose and lignin are still largely unchanged (Chen and Kuo 2011; Ben and Ragauskas 2012); the changes that do occur are limited to increases in both cellulose crystallinity and lignin cross-linking (Akgül et al. 2007; Bhuiyan et al. 2001; Melkior et al. 2012; Sivonen et al. 2002; Tjeerdsma et al. 1998). As the temperature rises to 300 °C, especially for extended periods of time, all of the cell wall polymers show significant degradation as evidenced by solid-state ^{13}C NMR spectroscopy (Ben and Ragauskas 2012; Melkior et al. 2012).

Numerous studies have shown the utility of coupling near-infrared (NIR) and/or Fourier transform infrared (FTIR) spectroscopic data with multivariate analysis to predict chemical, physical, and even mechanical properties for wood (Tsuchikawa and Schwanninger 2013; Gonzalez-Pena and Hale 2011). This has also been extended to wood charcoal where FTIR spectroscopic data showed principal component analysis (PCA) groupings between species and carbonization temperatures (Labbé et al. 2006); projection to latent structures (PLS) (also called partial least squares (PLS) regression) provided good predictions of the carbonization temperatures. Specific to torrefaction, Rousset et al. (2011a) applied PCA to FTIR spectra of torrefied bamboo, observing differences based on torrefaction temperature. Another study by Rousset et al. (2011b) used NIR spectroscopy coupled with

multivariate analysis to assess the effect of temperature and treatment duration for solid samples of beech wood. Proximate analysis (e.g., ash, volatiles) and higher heating value (HHV) data for torrefied loblolly pine, sweetgum, and switchgrass were modeled by Via et al. (2013) using both NIR and FTIR spectroscopic data. A study by Lestander et al. (2014) is different in that predictions of properties involved samples from torrefaction, pyrolysis, and gasification operations, all obtained at pilot-scale or commercial plants; a key recommendation from this work was the necessity of developing in-line techniques for monitoring of product composition measures (e.g., H/C ratio), thereby providing the necessary means to control the thermal processing operations. Compared with NIR spectroscopy, easier spectral interpretation with better peak resolution is achieved with FTIR spectroscopy, and ATR accessories allow rapid spectra collection with minimal sample preparation. FTIR spectroscopy has also been combined with thermogravimetric analysis (TGA) in the study of thermal degradation of biomass (Labbé et al. 2006; Zheng et al. 2015). Furthermore, combined TG-FTIR systems have been used to study, in real time, the reaction mechanisms and gases evolved during pyrolysis (Gao et al. 2013; Salema et al. 2014).

Multivariate analysis has also been applied to thermogravimetric data obtained from torrefied biomass for the prediction of mass yield from temperature data provided by differential thermogravimetric (DTG) decomposition curves (Strandberg et al. 2017); predictions of HHV, carbon, hydrogen, and oxygen were also obtained. It was also found that varying amounts of inorganic elements affected the PLS modeling (Strandberg et al. 2017). PCA has also been applied to the DTG curves. Groupings showed that substantial changes in the chemical composition and thermal properties provide separation between samples processed at the upper (275–300 °C) and lower (200–250 °C) temperature ranges for torrefaction (Barta-Rajnai et al. 2016).

Intuitively, any significant chemical changes to the cell wall polymers occurring during torrefaction should manifest significant differences in the biofuel properties (i.e., ultimate and proximate analysis data). Increasing the severity of the torrefaction conditions, as a function of the torrefaction temperature and/or treatment duration, results in increasing impacts on these data. Torrefaction product yield, measured by the recovery of solid material, is often overlooked but may provide a simple indicator of the degree of torrefaction from which operating parameters of temperature and/or time can be adjusted; mass yield is a function of chemical changes to the cell wall polymers and therefore should show correlations to the ultimate and proximate analysis data. The generation of a consistent torrefaction product, as well as the optimization of process conditions, remains a research need, particularly when taking into consideration the scale of the operation (Eseyin et al. 2015). Likewise, many studies are conducted using particle sizes that are impractical for commercial operations; thus, there is also the need to investigate the torrefaction of large particles (Ciolkosz and Wallace 2011).

A crucible furnace retort was fabricated with a sufficient capacity that would allow investigations of the impacts of operating parameters and wood feedstock conditions on the torrefaction of large wood particles, specifically pulp-grade wood chips (Eberhardt and Reed 2014); another factor considered in the design was

having sufficient capacity to generate enough solid carbonized product to conduct studies on alternative uses for torrefied wood, such as chemical feedstock production (Zhou et al. 2016). In the current study, the objective was to develop spectroscopy-based models for the rapid assessment of mass yield and biofuel properties on the torrefaction of a wood chip feedstock. Thus, air-dry loblolly pine chips were torrefied at different temperatures and treatment durations to generate samples with a wide range of mass yields. In addition to mass yield data, ultimate analysis (carbon, hydrogen, nitrogen content) and proximate analysis (HHV) data were collected for the development of predictive multivariate models based on FTIR spectroscopy. Principal component analysis was applied to the data to observe any differences between the samples and their processing conditions. Drying or grinding of the wood chip feedstock prior to torrefaction was found to impact conditions within the retort and thus mass yields. Spectra were also collected from these samples to assess whether the pretreatments would manifest in any spectral differences within the torrefied materials.

Materials and methods

Preparation of wood feedstocks

Pulp-grade pine wood chips, being clean wood with a species composition of mostly *Pinus taeda* L., were obtained from a local chip mill in Winnfield, LA, USA. Three sets of samples were prepared. The first sample of wood chips was dried under ambient conditions over several weeks in a laboratory environment. The second set of wood chips was obtained by drying a subset of the air-dry wood chips in a laboratory oven (103 ± 2 °C) until a constant oven-dry mass was achieved (i.e., 0% moisture content). The third set of wood chips, also a subset of the wood chips dried under ambient conditions, was ground in an electric chipper shredder (Echo, Inc., Model SH-5000) and then screened to give particles passing through an 8-mesh (2.4-mm openings) sieve and retained on a 20-mesh (0.85-mm openings) sieve. Particles were mostly slivers ranging from 2 to 20 mm in length; agitation during the sieving process was sufficient to allow long thin slivers to rise up on end and pass through the 8-mesh sieve.

Torrefaction of wood feedstocks

Wood chips/particles were then torrefied in a crucible furnace retort fabricated by Thermal Product Solutions (Williamsport, PA, USA); a basic schematic of the retort can be found in a report by Eberhardt and Reed (2014). Heating of the retort was accomplished with a programmable Lindberg Model 5661 crucible furnace having a Watlow EZ-Zone PM programmable integral derivative (PID) controller. Wood feedstocks (ca. 50 g, air-dry chips, oven-dry chips, air-dry particles) were kept within a high-form porcelain crucible (250 mL) placed in the bottom of the retort. The retort cover was installed with specific attention given to the placement of the outlet purge tube such that it was aligned past the side of the crucible. Under a

constant purge of N_2 (1 L min^{-1}), the retort was heated from ambient temperature to the targeted operating temperature. Wood feedstocks were torrefied using three different times (2, 3, and 4 h) and three different targeted operating temperatures (230, 260, and 290 °C). The time required to heat the retort to each of the three targeted operating temperatures (230, 260, and 290 °C) was approximately 1 h (heating rates ranging from 3.4 to 4.4 °C/min); no overshoot in temperature was observed (see Eberhardt and Reed 2014). The residence time at the targeted operating temperature was 1, 2, or 3 h; thus, the torrefaction time (2, 3, or 4 h) is defined as the time required to heat to operating temperature (1 h) in addition to the residence time (1, 2, or 3 h). When the torrefaction run was complete, the retort was removed from the furnace and placed on a stand to cool to room temperature before stopping the flow of N_2 and removing the sample-containing crucible. The time required to cool the internal temperature of the retort to 100 °C was 30 min (average cooling rate of − 5.3 °C/min) with an additional 1 h needed to reach room temperature (total cooling time = 1.5 h). Mass yields of torrefied wood were based on the dry weights of the torrefied wood and the starting wood feedstock. Samples were processed using 2 or 3 replicates for each temperature and run time combination, totaling 66 samples of torrefied wood. The exact number for each of the combinations is listed in Table 1. Torrefied wood chips were ground in a large Wiley mill equipped with a 4-mm milling screen. Subsamples used for FTIR spectroscopic and elemental analyses required further grinding in a small Wiley mill equipped with a 20-mesh (0.85 mm) milling screen.

Proximate and ultimate analyses

Moisture contents of the air-dry feedstocks (wood chips, wood particles) were determined by drying subsamples in a laboratory oven (103 ± 2 °C) until a constant dry mass was achieved. The moisture contents of the air-dry wood chips and particles were 9.6 and 8.3%, respectively; the difference between the two air-dry feedstocks was attributed to passive drying during grinding. A Parr oxygen bomb calorimeter 6100 (Parr Instruments, Moline, IL, USA) was used for higher heating value (HHV) determinations following the instructions in the manufacturer's operating manual (Parr Instruments 2006), using ca. 750 mg subsamples; this analysis was only performed on the torrefied wood samples produced from the air-dry wood chips. Carbon, hydrogen, and nitrogen contents were determined at a contract laboratory using a CHN analyzer (Fisons NA 1500, Danvers, MA, USA) using ca. 5 mg subsamples from material that had been ground further to pass a 40-mesh (0.42 mm) milling screen. Differences in standard replicates were generally less than 2%; thus, a typical carbon content of 50% would vary by ± 1% and a typical hydrogen content of 5% would vary by ± 0.1% (Table 1); however, there were also several larger variations among the replicates listed in Table 1. Nitrogen contents ranged from not detectable to ca. 0.1% and thus were not included in the results presented in this study.

Table 1 Averaged mass yield and analytical data for all combinations of torrefaction temperature and treatment duration (standard deviations shown in parentheses)

Temp (°C)	Time (h)	*N*	Carbon (%)	Hydrogen (%)	Mass yield (%)	HHV (MJ/kg)
Air-dry wood chips						
230	2	3	49.6 (1.0)	5.6 (0.2)	95.6 (0.2)	19.95 (0.49)
	3	2	52.0 (0.2)	5.7 (0.0)	93.0 (0.8)	20.46 (0.15)
	4	2	57.3 (0.4)	5.4 (0.1)	91.5 (0.4)	20.67 (1.21)
260	2	3	53.3 (0.7)	5.5 (0.1)	85.3 (1.9)	22.25 (1.15)
	3	2	58.4 (0.5)	4.9 (0.2)	82.8 (0.5)	22.03 (0.11)
	4	2	61.3 (0.3)	5.4 (0.1)	78.4 (0.0)	22.11 (0.58)
290	2	3	57.6 (0.8)	5.4 (0.1)	67.4 (1.3)	25.07 (0.26)
	3	2	75.7 (1.1)	5.0 (0.1)	61.6 (0.5)	26.38 (0.19)
	4	2	77.2 (2.4)	4.8 (0.1)	47.2 (3.6)	27.95 (0.11)
Oven-dry wood chips						
230	2	2	51.9 (0.9)	6.0 (0.0)	93.2 (1.4)	–
	3	2	52.5 (0.4)	5.8 (0.0)	91.6 (0.1)	–
	4	2	56.7 (0.5)	6.2 (0.1)	90.3 (0.4)	–
260	2	2	55.1 (0.1)	5.7 (0.0)	82.5 (0.2)	–
	3	2	55.6 (0.5)	5.6 (0.0)	79.4 (0.5)	–
	4	2	57.1 (0.1)	6.0 (0.0)	78.1 (0.7)	–
290	2	2	62.6 (0.0)	5.4 (0.0)	60.2 (1.1)	–
	3	2	68.7 (0.5)	5.0 (0.4)	54.0 (1.4)	–
	4	2	70.8 (0.4)	5.4 (0.0)	51.3 (1.2)	–
Air-dry wood particles						
230	2	3	58.9 (0.6)	6.1 (0.1)	92.6 (0.1)	–
	3	3	54.5 (0.5)	5.2 (0.0)	90.2 (0.1)	–
	4	3	52.7 (0.3)	5.7 (0.1)	88.8 (0.3)	–
260	2	3	58.2 (1.0)	5.2 (0.6)	80.3 (0.3)	–
	3	3	59.8 (0.3)	5.1 (0.0)	77.1 (1.0)	–
	4	3	56.9 (0.1)	5.7 (0.1)	75.0 (0.1)	–
290	2	3	72.0 (2.6)	4.7 (0.1)	55.1 (0.6)	–
	3	3	67.8 (2.0)	5.0 (0.1)	51.9 (1.3)	–
	4	3	68.2 (1.1)	5.1 (0.1)	49.9 (0.8)	–

Carbon and hydrogen contents of control (wood not torrefied) were 47.6% (SD = 0.3%) and 6.2% (SD = 0.2%), respectively

FTIR spectroscopy and data pretreatment

Spectra of the samples were collected in triplicate using a Nexus 670 FTIR spectrometer (Thermo Nicolet Instruments, Madison, WI, USA) equipped with a Golden Gate MKII Single Reflection ATR accessory. The spectral region was 4000–650 cm^{-1} using a spectral resolution of 4 cm^{-1} and 32 scans per sample.

Multivariate analysis of the spectral data was performed using the Unscrambler (version 8.0) software (CAMO, Woodbridge, NJ, USA). The FTIR data collected were first mean-normalized and then averaged to one spectrum per sample. Several data pretreatment techniques were also applied to the spectra, along with the raw data, including first derivatives (Savitzky–Golay 5-point averaging) and multiplicative scatter correction (MSC) to reduce the effect of noise in the spectral data (Næs et al. 2002).

Multivariate modeling and diagnostics

Principal component analysis (PCA) (Wold et al. 1987) was performed on the spectral data to observe any differences and groupings between the samples. Partial least squares (PLS) regression (Wold 1975) was used to predict mass yield as well as carbon and hydrogen contents. Calibration and test sets were randomly generated using two-thirds ($N = 44$) and the remaining one-third ($N = 22$) of the total samples ($N = 66$), respectively. Models were generated using cross-validation (with mean centering) and assessed via several common measures of calibration performance, including multiple coefficient of determination (R^2), root-mean-square error of cross-validation (RMSECV) as determined from the residuals of each cross-validation phase, and the root-mean-square error of prediction (RMSEP) as determined from the residuals of the prediction. The equations for these parameters are provided in Næs et al. (2002).

Results and discussion

Torrefaction of wood feedstocks

The average mass yields of torrefied wood are shown in Table 1. Increasing the temperature and/or the time resulted in darker sample colorations and lower mass yields (i.e., higher torrefaction severity), though to a much lesser extent as a function of time than temperature; higher losses of mass are the result of higher degrees of thermal degradation of the cell wall polymers to volatile products (Prins et al. 2006c), these being purged from the retort by the flow of nitrogen. Since torrefaction for 2 h at 230 °C gave mass yields of ca. 93–96%, shorter torrefaction times were not pursued. The average mass yield from the torrefaction of air-dry wood chips for 5 h at 290 °C was 50.14 ± 0.81%, a value that was essentially equivalent to that obtained for 4 h at the same temperature (Table 1). Since the degree of thermal degradation appeared to level off, torrefaction times longer than 4 h were not pursued. Altogether, the wide range of mass yields was anticipated to reflect a wide spectrum of chemical changes resulting from varying degrees of thermal degradation. The high mass yields for the lowest temperature (230 °C) likely represent torrefied woods for which minimal levels of thermal degradation occurred, primarily with the hemicelluloses. While both higher torrefaction temperatures and longer torrefaction times (at a given temperature) lead to lower mass yields, torrefaction temperature has been shown to have a greater effect on

torrefaction degree than time (Strandberg et al. 2015; Rudolfsson et al. 2017). Thus, torrefaction temperature and time were not totally interchangeable when applying multiple linear regression models for several properties, such as HHV (Strandberg et al. 2015); it was concluded that further work would be needed to determine the number of properties which could be used such that one temperature–time combination could be exchanged for another combination.

Mass yields of torrefied wood for the oven-dry (i.e., 0% moisture content) wood chips averaged 3.1% lower than those for the air-dry wood chips. Temperature monitoring during the various torrefaction cycles demonstrated that moisture in the air-dry wood chips (moisture content = 9.6%) reduced the rate of retort heating compared to the rate observed with either an empty retort or when processing oven-dry wood chips (Eberhardt and Reed 2014). Thus, the higher heating rate afforded by predrying the wood chips led to greater residence time at higher temperatures leading to greater thermal degradation (i.e., lower mass yields). The exceptions were at the extreme conditions (4 h at both 260 and 290 °C) whereby the extended time compensated for any lag in temperature increase during the heating phase of the process.

In a review by Ciolkosz and Wallace (2011), the use of large particles (e.g., wood chips) for torrefaction was stated to be a research need, the rationale being that torrefaction yields/products from a given feedstock are a function of time, temperature, and particle size. Torrefaction of the air-dry wood particles (8–20 mesh) gave lower mass yields than both the air- and oven-dry wood chips. The greatest difference was at the torrefaction temperature of 290 °C with a total treatment time of 2 h; the mass yields for the air-dry wood chips and air-dry wood particles were 67.4 and 55.1%, respectively (Table 1). Greater heat transfer increases the rate of thermal degradation, but perhaps more importantly facilitates moisture loss. Thus, both oven drying or grinding wood chips prior to torrefaction resulted in lower mass yields. Larger wood chip sizes likely impede water release, thereby reducing the rate of thermal degradation and resulting in higher mass yields.

Proximate and ultimate analyses

Van Krevelen diagrams provide information about the hydrogen/carbon ratio relative to the oxygen/carbon ratio and can be used to compare fuel types with both ratios being higher for biomass feedstocks than carbon-rich fuels like coal (van der Stelt et al. 2011); torrefaction of wood moves it in the plot to a position somewhat closer to coal through the losses in both oxygen and hydrogen via volatile degradation products, thus resulting in carbon enrichment. The elemental analysis in this current study clearly showed that the carbon content increased and the hydrogen content decreased with temperature (Table 1), as expected for increasingly severe torrefaction conditions (Na et al. 2013). Comparing the averaged values at the extreme temperatures (230 vs. 290 °C), for all torrefaction times, the increases in carbon content for the air-dry and oven-dry wood chips were 25 and 33%, respectively. Carrying out a similar comparison for the hydrogen contents, the decreases in hydrogen content for the air-dry and oven-dry samples were 13 and 8.9%, respectively. The most severely torrefied samples available for further

evaluation were the air-dry wood chips torrefied at 290 °C for 4 h. This resulted in the highest carbon content (77.2%) accompanied by a low hydrogen content (4.8%) at the lowest mass yield (47.2%). The air-dry wood chips torrefied at 230 °C for 2 h resulted in the samples with the lowest carbon content (49.6%) accompanied by a high hydrogen content (5.6%) at the highest mass yield (95.6%). Similar to other studies (Na et al. 2013), nitrogen contents were also determined to be low (ca. 0.1%) in value and invariable (data not shown). Ash contents were not determined given that the concentration of inorganic compounds is without question and the ash content of the wood chip feedstock was low (0.32%); thus, with mass yields as reported here, the ash contents of the torrefaction products would be quite low and in a narrow range (ca. 0.34 to ca. 0.68%).

One benefit of torrefying wood for bioenergy applications is an increase in energy density based on weight (van der Stelt et al. 2011). Thus, increases in torrefaction severity were expected to result in increases in the higher heating value (HHV). Calorimetry was performed on the torrefied air-dry wood chips and gave results consistent with decreasing mass yields, increasing carbon contents, and decreasing hydrogen contents. The inverse relationship of mass yield to HHV was examined and found to be linear (Fig. 1) with a R^2 value of 0.95 and a low standard error of estimation (SEE) of 0.73 MJ/kg (Table 2). The linear correlation between HHV and the individual elements of carbon and hydrogen is reported in Table 2 showing the stronger correlation with carbon ($R^2 = 0.71$) than with hydrogen ($R^2 = 0.44$). Lestander et al. (2014) obtained a high correlation ($R^2 = 0.99$) with ash-free carbon content when applying a second-order polynomial fit to mass yield. Since HHV shows relationships to elemental composition, equations with carbon and hydrogen (as well as nitrogen) as variables have been used to calculate HHV for various biomass feedstocks (Gaur and Reed 1995; Demirbas and Demirbas 2004).

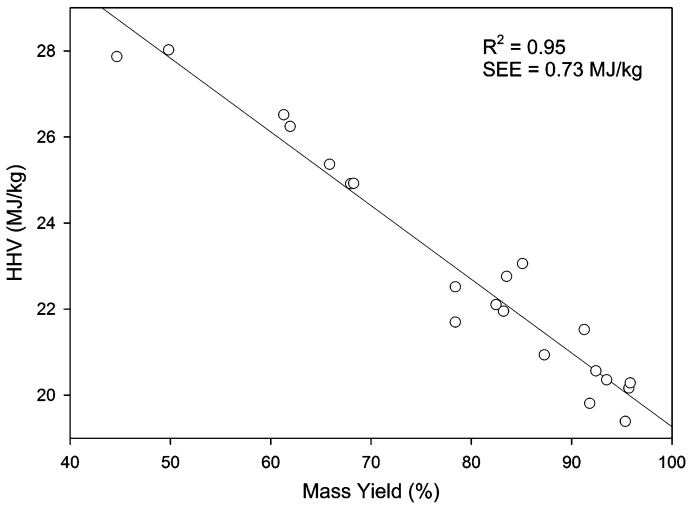

Fig. 1 Relationship between mass yield and HHV for air-dry wood chips torrefied at 230, 260, and 290 °C

Table 2 Statistics for selected linear regressions between HHV, mass yield, carbon, and hydrogen

	Sample	*N*	R^2	SEE
HHV versus mass yield			0.95	0.73 MJ/kg
HHV versus carbon	Air-dry wood chips	21	0.70	2.13 MJ/kg
HHV versus hydrogen			0.48	7.54 MJ/kg
Mass yield versus carbon	All samples	66	0.71	9%
	Air-dry wood chips	21	0.75	11%
	Oven-dry wood chips	18	0.69	9%
	Air-dry wood particles	27	0.86	6%
Mass yield versus hydrogen	All samples	66	0.44	19%
	Air-dry wood chips	21	0.55	40%
	Oven-dry wood chips	18	0.67	9%
	Air-dry wood particles	27	0.44	12%

Similar with HHV, the relationships between mass yield with carbon and mass yield with hydrogen were also examined, in which the R^2 values for the air-dry wood chips were found to be fairly similar to those from the HHV correlation. Furthermore, the effect of particle size was investigated showing that the best correlation between mass yield and carbon was obtained from the smaller wood particles with a R^2 of 0.86 (Table 2). The best correlations for mass yield with hydrogen were obtained from the oven-dry wood chips ($R^2 = 0.67$). Similarly, mass loss has been used to predict energy properties, obtaining excellent linear regressions for calorific content, fixed carbon, volatile matter, and energy yield (Almeida et al. 2010; Pierre et al. 2011).

FTIR spectroscopy and band assignments

FTIR spectra were collected from all torrefied samples. For the purpose of direct comparison, Fig. 2a shows the averaged spectra (4000–650 cm^{-1} region) for the air-dry wood chips treated for 2 h at each torrefaction temperature (230, 260 or 290 °C). It was observed that as the torrefaction temperature was increased, the intensity of the broad band centered close to 3328 cm^{-1} decreased relative to a control sample of wood that was not subjected to torrefaction. Stelte et al. (2011) reported that the broad band at 3600–3200 cm^{-1}, associated with the O–H stretching vibration region, as well as the number of intra- and inter-molecular hydrogen bonds, becomes weaker with increasing temperature due to the degradation of hemicellulose and cellulose (Kymäläinen et al. 2015); at the torrefaction temperature of 300 °C, these bands were essentially absent. In that particular study, reduced capacity for hydrogen bonding led to the beneficial hydrophobicity observed in torrefied wood pellets, also discussed by Rudolfsson et al. (2017). The C-H band centered near 2900 cm^{-1} was also observed to broaden and weaken with increasing temperature.

Closer examination in the fingerprint region (1800–650 cm^{-1}) of the FTIR spectra in Fig. 2b shows that the samples from the 230 and 260 °C torrefaction

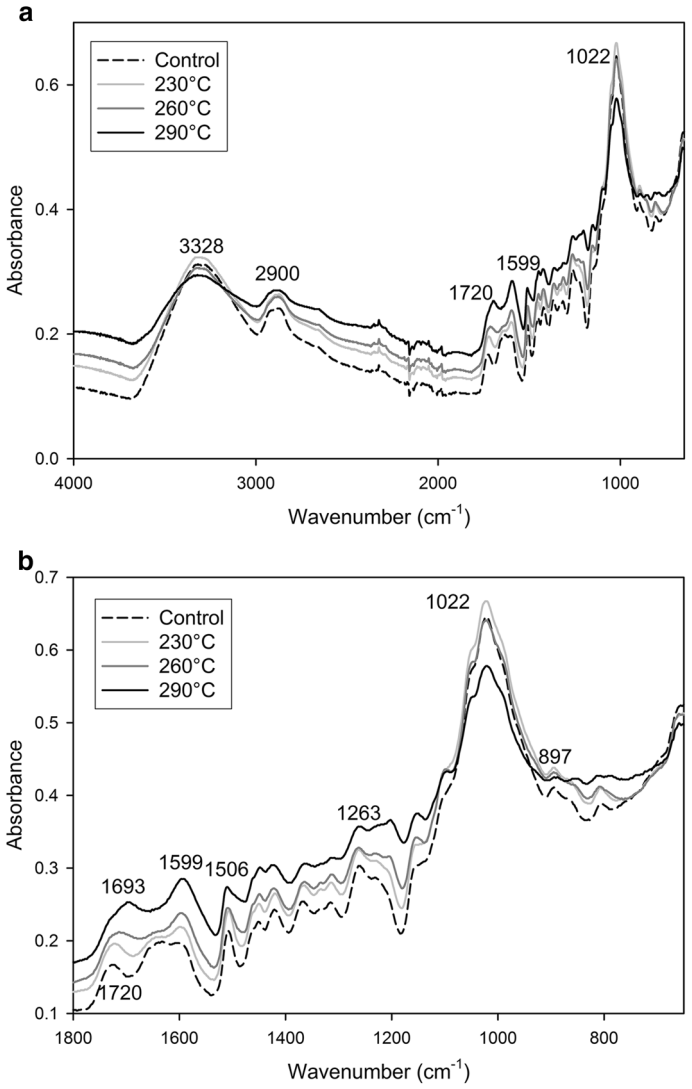

Fig. 2 **a** Averaged FTIR spectra (4000–650 cm^{-1}) for control (wood not torrefied) and air-dry wood chips torrefied for 2 h at 230, 260, and 290 °C. **b** Averaged FTIR spectra (1800–650 cm^{-1}) for the control (wood not torrefied) and air-dry wood chips torrefied for 2 h at 230, 260, and 290 °C

temperatures, and the above-mentioned control (wood not torrefied), gave relatively similar spectra. In comparison, the spectrum for the 290 °C torrefaction temperature shows significantly weaker bands. This observation parallels that by Stelte et al. (2011) where the spectrum for wood torrefied at 300 °C was distinctly different to the relatively similar spectra for control wood and that torrefied at temperatures of 250 and 275 °C. It can be observed that the C=O stretching band at 1720 cm^{-1} broadens and shifts to lower wavenumbers (1693 cm^{-1} at 290 °C) as a result of

hemicellulose and cellulose degradation occurring between 250 and 280 °C (Rousset et al. 2011a; Park et al. 2013). Lignin vibrations, with bands present at 1263 cm^{-1} (aromatic C–O stretching of methoxyl units) and 1506 cm^{-1} (aromatic C=C ring vibration), decrease at high temperatures as lignin degrades (Stelte et al. 2011; Zheng et al. 2015). Other spectral changes in the lignin-related bands include the stretching C=C vibration peak at 1599 cm^{-1} becoming increasingly pronounced. The prominent C–O band at 1022 cm^{-1} is assigned to cellulose and hemicelluloses and can be seen to decrease in intensity with increasing temperature (Park et al. 2013; Rousset et al. 2011a; Zheng et al. 2015). Pushkin et al. (2015) reported the disappearance of the 897 cm^{-1} band in Fig. 2b, attributed to amorphous cellulose, is associated with the increase in cellulose crystallinity. Expanding upon the spectral variations, more complex data manipulations were then employed, therein applying multivariate analysis to the complete set of spectra.

PCA and PLS models

Principal component analysis (PCA) was carried out using the FTIR spectra from the torrefied wood samples covering all temperatures, times, and torrefaction process feedstocks (i.e., air- and oven-dry chips, particles). Various pretreatments were applied to the FTIR spectra, in which normalized data provided the clearest sample separations in the scores plot, especially when employing the full spectral range (4000–650 cm^{-1}). The PCA scores plot in Fig. 3a shows the data to cluster along first principal component (PC 1) based on torrefaction temperature. The samples exposed to the lowest temperatures (230 and 260 °C) are located on the positive side of PC 1, while those with the highest temperature (290 °C) are located on the negative side of PC 1, with this principal component accounting for 93% of the total spectral variance; the second principal component (PC 2) accounted for 5% of the total spectral variance. Clustering according to temperature has been previously observed with oak and maple samples heated to temperatures between 250 and 350 °C (Labbé et al. 2006) and bamboo heated to 220–280 °C (Rousset et al. 2011a). The latter of these two studies (i.e., the bamboo study) noted greater scatter in the data for the highest torrefaction temperature (280 °C), which was attributed to lignin degradation. In the present study, the same pattern is observed in which the wood feedstocks torrefied at 290 °C show much greater scattering, along PC 1, than those at the lower temperatures (Fig. 3a). In addition, the distribution of the data points for the samples torrefied at 290 °C appear to show some clustering relative to treatment time for each sample set. The torrefied wood samples from the air-dry chip feedstock (triangles a2–a4) show the largest variation along PC 1 for the three torrefaction times, with the longer torrefaction times located further along the negative side of PC 1. The same is observed with the torrefied wood samples from the oven-dry wood chips (triangles o2–o4) and the air-dry wood particles (circles a2–a4), but to a lesser degree. This data pattern is not discernible for the other torrefaction temperatures with the tighter clustering of the data along the positive side of PC 1. The scores plot in Fig. 3a also showed separation based on particle size, in which the wood particles (circles) are located on the positive side of PC 2, while the wood chips (triangles) are located on the negative side of PC 2. Thus, PCA

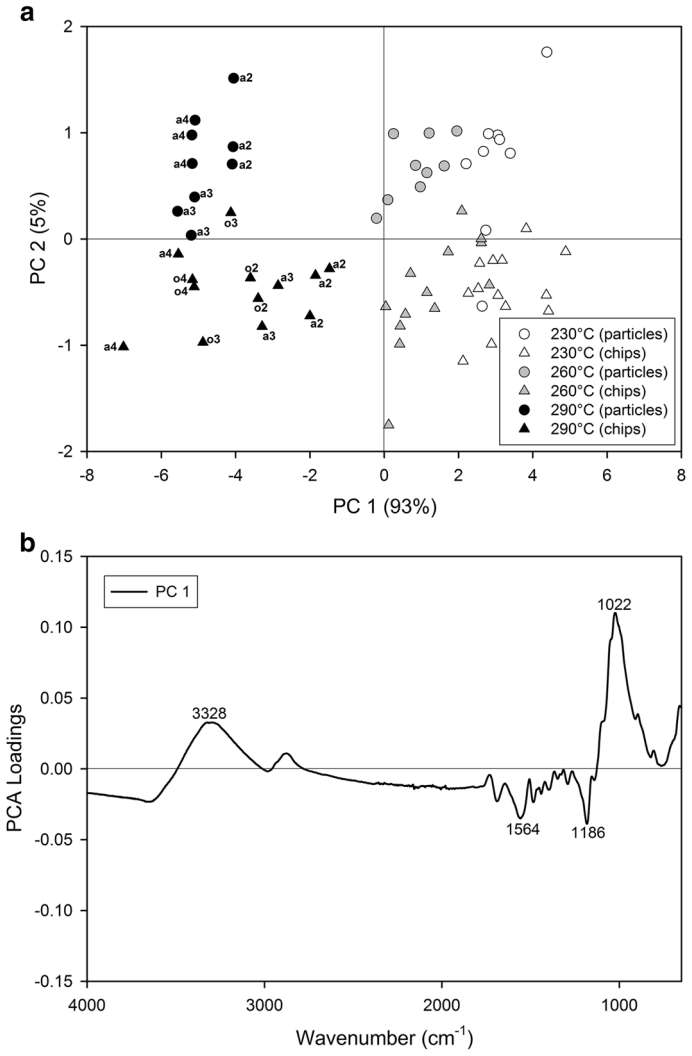

Fig. 3 **a** PCA scores plot from the FTIR spectra for all ($N = 66$) samples showing torrefaction temperature and particle size, using normalized spectra. For the 290 °C samples (black shapes): air-dry (a); oven-dry (o) and torrefaction times (2, 3, 4) in hours. **b** PC 1 loadings plot for the PCA scores plot in **a**

is detecting differences in the FTIR spectra between the wood chips and particles following torrefaction, as all samples were ground to the same particle size for spectra collection. Like with torrefaction time, the effects of the drying conditions of the wood chips were best observed with the feedstocks torrefied at 290 °C. This does show torrefied wood samples from the oven-dry wood chips (triangles o2–o4) further along the negative side of PC 1 than those from the air-dry wood chips (triangles a2–a3), apart from those at 4 h (triangles a4). Upon further investigation, the data point positions along PC1 for the air- and oven-dry wood chips (black

triangles), torrefied at 290 °C, appear to correspond with the mass yield values in Table 1. Specifically, for the wood chips torrefied at 290 °C, it appears that as one moves further along the negative side of PC 1, the lower will be the mass yield. This is not surprising as mass yield decreases with increasing torrefaction temperature. The unexpected large mass yield drop for the air-dry chips at 290 °C for 4 h shown in Table 1 is visually observed by the location of the samples (triangles a4) in the scores plot (Fig. 3a).

The PC 1 loadings plot from the PCA scores plot is shown in Fig. 3b and highlights the chemical features contributing to the separation along PC 1; wavenumbers with large loadings, both positive and negative, are those that contribute most to the variation in the scores plot along PC 1. The PC 1 loadings plot shown here is similar to that reported for a series of wood charcoals (Labbé et al. 2006), although the magnitude of the loadings are slightly different. The scores plot in Fig. 3a indicates that the separation along PC 1 is primarily based on temperature. In the PC1 loadings plot (Fig. 3b), the large positive loading around 1022 cm^{-1} is associated with the C–O stretching vibration indicating a decrease in cellulose and hemicellulose with an increase in temperature. Thus, the lower-temperature (230 and 260 °C) samples, located on the positive side of PC 1 in Fig. 3a, have relatively higher cellulose and hemicellulose content than samples at the higher temperature (Labbé et al. 2006; Rousset et al. 2011a). Likewise, with the negative loadings of the 1564 and 1186 cm^{-1} lignin bands, it is surmised that the high-temperature (290 °C) samples, located on the negative side of PC 1 in Fig. 3a, have a relatively higher lignin content (Labbé et al. 2006). The positive loading of the broad O–H band centered around 3328 cm^{-1} also appears to be more prevalent with the lower-temperature samples. The loadings plot for PC 2 (not shown), provided separation between chips and particles in the scores plot, was primarily due to a negative broad O–H band.

Partial least squares regression was performed to assess the potential to predict mass yield, along with carbon and hydrogen contents, from the FTIR spectra. Calibration models were built using two samples sets: the total (All) sample set using all 66 samples and the calibration (Calib) sample set using only 44 of the samples. The strength of the Calib model was tested using a separate (Test) sample set using the remaining 22 samples not used in the Calib sample set; note that these test set samples were not fully independent from the calibration set. Statistics for the variation within these sample sets are listed in Table 3, in which the max and min values were obtained from individual samples, rather than the averages for each time and temperature combination as given in Table 1. The regressions were performed on the raw spectra, first-derivative, and MSC-treated spectra. The models based on the raw spectral data utilized more factors to provide similar results to those from the treated spectral data for mass yield, carbon and hydrogen content (Table 3). The best models, for all treatments, were clearly built with mass yield. High R^2 values were obtained from both calibration and test sets, using only two factors, for both MSC and first-derivative spectra. The RMSECV and RMSEP values for the MSC-based models were notably better than that for the first-derivative-based models. Figure 4a shows the predicted versus measured mass yield plot for the calibration and test models using MSC-treated spectra. The high-temperature samples at 290 °C (diamonds), with low mass yields, exhibit greater

Table 3 PLS regression statistics for mass yield, carbon, and hydrogen of the predictions; here these two errors are denoted RMSECV/RMSEP; RMSECV for the all and calibration sets and RMSEP for the test set

Samples	*N*	Max	Min	Mean	SD	Treatment	Factors	RMSECV/RMSEP	R^2
Mass yield (%)									
All	66	95.8	44.7	75.7	15.8		4	2.03	0.98
Calib	44	95.7	44.7	75.2	16.9	Raw	4	1.99	0.99
Test	22	95.8	50.3	76.8	13.7		4	1.72[a]	0.99
All	66	95.8	44.7	75.7	15.8		2	2.20	0.98
Calib	44	95.7	44.7	75.2	16.9	1st deriv.	2	2.34	0.98
Test	22	95.8	50.3	76.8	13.7		2	2.37	0.97
All	66	95.8	44.7	75.7	15.8		2	2.02	0.98
Calib	44	95.7	44.7	75.2	16.9	MSC	2	1.82	0.99
Test	22	95.8	50.3	76.8	13.7		2	1.64[a]	0.99
C (%)									
All	66	81.0	48.6	59.4	7.5		2	4.19	0.68
Calib	44	78.9	48.6	59.0	7.4	Raw	2	3.62	0.76
Test	22	81.0	50.6	60.1	7.8		2	5.26	0.61
All	66	81.0	48.6	59.4	7.5		1	4.11	0.69
Calib	44	78.9	48.6	59.0	7.4	1st deriv.	1	3.54	0.77
Test	22	81.0	50.6	60.1	7.8		1	5.56	0.53
All	66	81.0	48.6	59.4	7.5		1	4.10	0.71
Calib	44	78.9	48.6	59.0	7.4	MSC	1	3.26	0.82
Test	22	81.0	50.6	60.1	7.8		1	5.56	0.56
H (%)									
All	66	6.2	4.6	5.4	0.4		2	0.35	0.33
Calib	44	6.2	4.7	5.4	0.4	Raw	2	0.32	0.36
Test	22	6.2	4.6	5.5	0.5		2	0.39	0.32
All	66	6.2	4.6	5.4	0.4		1	0.33	0.38
Calib	44	6.2	4.7	5.4	0.4	1st deriv.	1	0.31	0.40
Test	22	6.2	4.6	5.5	0.5		1	0.40	0.27
All	66	6.2	4.6	5.4	0.4		1	0.33	0.42
Calib	44	6.2	4.7	5.4	0.4	MSC	1	0.30	0.46
Test	22	6.2	4.6	5.5	0.5		1	0.38	0.35

[a]Most often RMSEP is larger than RMSECV

scatter about the equivalence line than the lower-temperature samples. Figure 4b is the corresponding regression coefficient plot showing that wavelengths in the 1800–650 cm^{-1} region are contributing most to the mass yield calibration model. There are several bands that show a negative correlation with the model, of which the lignin band at 1186 cm^{-1} clearly has the largest effect, followed by the C=O band at 1693 cm^{-1}, and the lignin band at 1599 cm^{-1}.

Partial least squares regression models were also built to predict carbon and hydrogen content (Table 3). The calibration models for carbon content provided

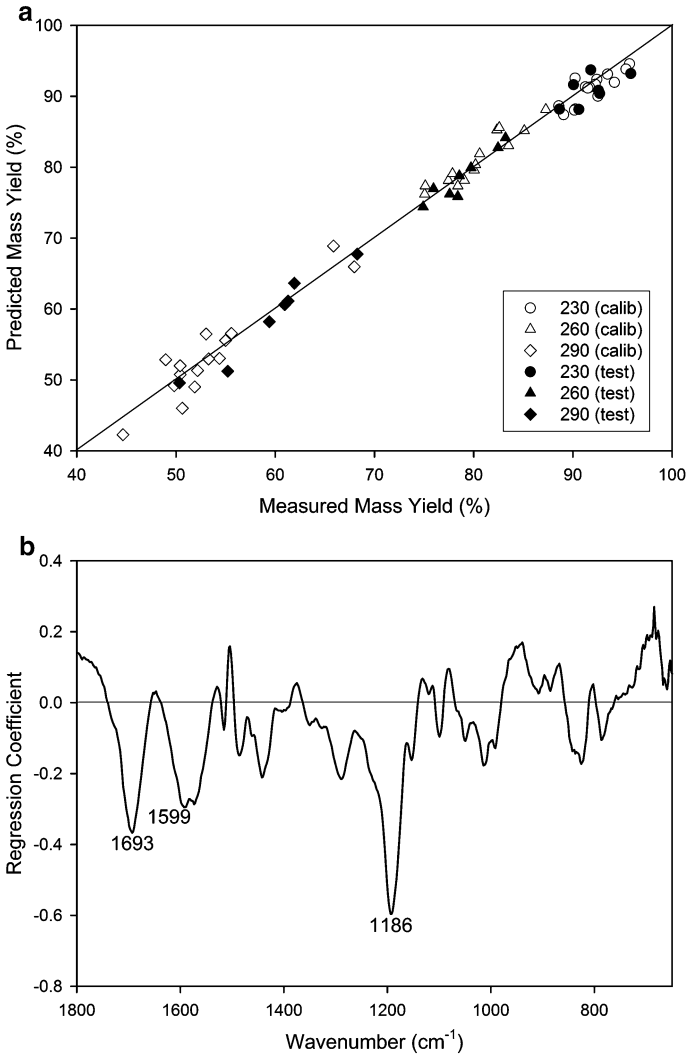

Fig. 4 **a** PLS predicted versus measured plot for mass yield for the calibration ($N = 44$) and test ($N = 22$) sets samples showing torrefaction temperature, using MSC-treated spectra. **b** Regression coefficients from the PLS model for mass yield in **a**

weaker R^2 values with reasonable RMSECV values for the first-derivative and MSC-treated spectra; however, the predictive abilities from the test sets were not particularly strong. The models for hydrogen content were poor, undoubtedly reflecting the ranges for the analytical values, with the hydrogen content falling within a tight set of values (4.6–6.2%). The software recommended using one factor for the regressions based on the treated spectra. Increasing the number of factors did not lower the RMSEP values. Altogether, FTIR monitoring coupled with PLS

regressions would appear to provide a reliable rapid assessment technique to predict mass yield and to a lesser extent carbon content.

Conclusion

This study showed that both oven drying and grinding of wood chips prior to torrefaction provided lower mass yields, via greater heat transfer and moisture loss. Ultimate analysis showed that carbon had strong relationships with both mass yield and HHV, which in themselves have a high correlation. Differences were observed in the FTIR spectra, which were clearly observed in the PCA, providing separation in terms of torrefaction temperature, time, and sample type (i.e., with or without pretreatments of grinding or drying). The degradation in hemicellulose, followed by lignin and cellulose was evident by the chemical bands assigned to these constituents. Mass yields can also be readily predicted from the FTIR spectra, with the PCA loadings plot showing the chemical bands that provide the high correlation. The application of FTIR spectroscopy to wood torrefaction can be used as a rapid assessment technique to determine mass yield, such as in a production environment where mass yield is related to product quality parameters such as HHV and carbon content.

Acknowledgements This material is based upon work that is supported by the National Institute of Food and Agriculture, US Department of Agriculture, Hatch Project Under LAB04545.

References

Akgül M, Gümüskaya E, Korkut S (2007) Crystalline structure of heat-treated Scots pine (*Pinus sylvestris* L.) and Uludağ fir (*Abies nordmanniana* (Stev.) subsp. *bornmuelleriana* (Mattf.)) wood. Wood Sci Technol 41:281–289

Almeida G, Brito JO, Perré P (2010) Alterations in energy properties of eucalyptus wood and bark subjected to torrefaction: the potential of mass loss as a synthetic indicator. Bioresour Technol 101:9778–9784

Arias B, Pevida C, Fermoso J, Plaza MG, Rubiera F, Pis JJ (2008) Influence of torrefaction on the grindability and reactivity of woody biomass. Fuel Process Technol 89:169–175

Barta-Rajnai E, Jakab E, Sebestyén Z, May Z, Barta Z, Wang L, Skreiberg O, Grønli M, Bozi J, Czégény Z (2016) Comprehensive compositional study of torrefied wood and herbaceous materials by chemical analysis and thermoanalytical methods. Energy Fuels 30:8019–8030

Ben H, Ragauskas AJ (2012) Torrefaction of loblolly pine. Green Chem 14:72–76

Bhuiyan MTR, Hirai N, Sobue N (2001) Effect of intermittent heat treatment on crystallinity in wood cellulose. J Wood Sci 47:336–341

Bridgeman TG, Jones JM, Shield I, Williams PT (2008) Torrefaction of reed canary grass, wheat straw and willow to enhance solid fuel qualities and combustion properties. Fuel 87:844–856

Chen W-H, Kuo P-C (2011) Torrefaction and co-torrefaction characterization of hemicellulose, cellulose and lignin as well as torrefaction of some basic constituents in biomass. Energy 36:803–811

Chew JJ, Doshi V (2011) Recent advances in biomass pretreatment—torrefaction fundamentals and technology. Renew Sustain Energy Rev 15:4212–4222

Ciolkosz D, Wallace R (2011) A review of torrefaction for bioenergy feedstock production. Biofuel Bioprod Biorefining 5:317–329

Couhert C, Salvador S, Commandré J-M (2009) Impact of torrefaction on syngas production from wood. Fuel 88:2286–2290

Demirbas A, Demirbas AH (2004) Estimating the calorific values of lignocellulosic fuels. Energy Explor Exploit 22(2):135–143
Deng J, Wang G-J, Kuang J-H, Zhang Y-L, Luo Y-H (2009) Pretreatment of agricultural residues for co-gasification via torrefaction. J Anal Appl Pyrol 86:331–337
Eberhardt TL, Reed KG (2014) Technical note: evaluation of a crucible furnace retort for laboratory torrefactions of wood chips. Wood Fiber Sci 46(4):600–604
Eseyin AE, Steele PH, Pittman CU Jr (2015) Current trends in the production and applications of torrefied wood/biomass—a review. BioResources 10(4):8812–8858
Gao N, Li A, Quan C, Dub L, Duan Y (2013) TG–FTIR and Py–GC/MS analysis on pyrolysis and combustion of pine sawdust. J Anal Appl Pyrol 100:26–32
Gaur S, Reed T (1995) An atlas of thermal data for biomass and other fuels. NREL/TB-433-7965, UC category: 1310, DE95009212, National Renewable Laboratory, Golden Colorado, USA
Gonzalez-Pena MM, Hale MDC (2011) Rapid assessment of physical properties and chemical composition of thermally modified wood by mid-infrared spectroscopy. Wood Sci Technol 45:83–102
Kymäläinen M, Rautkari L, Hill CAS (2015) Sorption behavior of torrefied wood and charcoal determined by dynamic vapour sorption. J Mater Sci 50:7673–7680
Labbé N, Harper D, Rials T, Elder T (2006) Chemical structure of wood charcoal by infrared spectroscopy and multivariate analysis. J Agric Food Chem 54:3492–3497
Lestander TA, Rudolfsson M, Pommer L, Nordin A (2014) NIR provides excellent predictions of properties from torrefaction and pyrolysis of biomass. Green Chem 16:4906–4913
Li H, Liu X, Legros R, Bi XT, Lim CJ, Sokhansanj S (2012) Pelletization of torrefied sawdust and properties of torrefied pellets. Appl Energy 93:680–685
Medic D, Darr M, Shah A, Potter B, Zimmerman J (2012) Effects of torrefaction process parameters on biomass feedstock upgrading. Fuel 91:147–154
Melkior T, Jacob S, Gerbaud G, Hediger S, Le Pape L, Bonnefois L, Bardet M (2012) NMR analysis of the transformation of wood constituents by torrefaction. Fuel 92(1):271–280
Meng J, Park J, Tilotta D, Park S (2012) The effect of torrefaction on the chemistry of fast-pyrolysis bio-oil. Bioresour Technol 111:439–446
Na BI, Kim YH, Lim WS, Lee SM, Lee HW, Lee JW (2013) Torrefaction of oil palm mesocarp fiber and their effect on pelletizing. Biomass Bioenerg 52:159–165
Næs T, Isaksson T, Fearn T, Davies T (2002) A user-friendly guide to multivariate calibrations and classification. NIR Publications, Chichester
Park J, Meng J, Lim KH, Rojas OJ, Park S (2013) Transformation of lignocellulosic biomass during torrefaction. J Anal Appl Pyrol 100:199–206
Parr Instruments (2006) Parr 6100 operating manual, version date 9-6-06. Parr Instruments, Moine
Pierre F, Almeida G, Otavio Brito J, Perre P (2011) Influence of torrefaction on some chemical and energy properties of maritime pine and pedunculate oak. BioResources 6(2):1204–1218
Prins MJ, Ptasinski KJ, Janssen FJJG (2006a) More efficient biomass gasification via torrefaction. Energy 31:3458–3470
Prins MJ, Ptasinski KJ, Janssen FJJG (2006b) Torrefaction of wood Part 1. Weight loss kinetics. J Anal Appl Pyrol 77:28–34
Prins MJ, Ptasinski KJ, Janssen FJJG (2006c) Torrefaction of wood Part 2. Analysis of products. J Anal Appl Pyrol 77:35–40
Pushkin SA, Kozlova LV, Makarov AA, Grachev AN, Gorshkova TA (2015) Cell wall components in torrefied softwood and hardwood samples. J Anal Appl Pyrol 116:102–113
Rousset P, Aguiar C, Labbé N, Commandre J-M (2011a) Enhancing the combustible properties of bamboo by torrefaction. Bioresour Technol 102:8225–8231
Rousset P, Davrieux F, Macedo L, Perre P (2011b) Characterisation of the torrefaction of beech wood using NIRS: combined effects of temperature and duration. Biomass Bioenerg 35:1219–1226
Rudolfsson M, Stelte W, Lestander TA (2015) Process optimization of combined biomass torrefaction and pelletization for fuel pellet production—a parametric study. Appl Energy 140:378–384
Rudolfsson M, Borén E, Pommer L, Nordin A, Lestander TA (2017) Combined effects of torrefaction and pelletization parameters on the quality of pellets produced from torrefied biomass. Appl Energy 191:414–424
Salema AA, Afzal MT, Motasemi F (2014) Is there synergy between carbonaceous material and biomass during conventional pyrolysis? A TG-FTIR approach. J Anal Appl Pyrol 105:217–226

Sivonen H, Maunu SL, Sundholm F, Jämsä S, Viitaniemi P (2002) Magnetic resonance studies of thermally modified wood. Holzforschung 56:648–654

Stelte W, Clemons C, Holm JK, Sanadi AR, Ahrenfeldt J, Shang L, Henriksen UB (2011) Pelletizing properties of torrefied spruce. Biomass Bioenerg 35:4690–4698

Strandberg M, Olofsson I, Pommer L, Wiklund-Lindström S, Åberg K, Nordin A (2015) Effects of temperature and residence time on continuous torrefaction of spruce wood. Fuel Process Technol 134:387–398

Strandberg A, Holmgren P, Broström M (2017) Predicting fuel properties of biomass using thermogravimetry and multivariate data analysis. Fuel Process Technol 156:107–112

Tjeerdsma BF, Boonstra M, Pizzi A, Tekely P, Militz H (1998) Characterisation of thermally modified wood: molecular reasons for wood performance improvement. Holz Roh Werkst 56:149–153

Tsuchikawa S, Schwanninger M (2013) A review of recent near-infrared research for wood and paper (Part 2). Appl Spectrosc Rev 48:560–587

van der Stelt MJC, Gerhauser H, Kiel JHA, Ptasinski KJ (2011) Biomass upgrading by torrefaction for the production of biofuels: a review. Biomass Bioenerg 35:3748–3762

Via BK, Adhikari S, Taylor S (2013) Modeling for proximate analysis and heating value of torrefied biomass with vibration spectroscopy. Bioresour Technol 133:1–8

Wannapeera J, Fungtammasan B, Worasuwannarak N (2011) Effects of temperature and holding time during torrefacton on the pyrolysis behaviors of woody biomass. J Anal Appl Pyrol 92:99–105

Werner K, Pommer L, Broström M (2014) Thermal decomposition of hemicelluloses. J Anal Appl Pyrol 110:130–137

Wold H (1975) Path models with latent variables: the NIPALS approach. In: Blalock HM (ed) Quantitative sociology. Academic Press, New York, pp 305–357

Wold S, Esbensen K, Geladi P (1987) Principal component analysis. Chemometr Intell Lab Syst 2:37–52

Zheng A, Jiang L, Zhao Z, Huang Z, Zhao K, Wei G, Wang X, He F, Li H (2015) Impact of torrefaction on the chemical structure and catalytic fast pyrolysis behavior of hemicellulose, lignin, and cellulose. Energy Fuels 29:8027–8034

Zhou M, Eberhardt TL, Xin P, Hse C-Y, Pan H (2016) Liquefaction of torrefied wood using microwave irradiation. Energy Fuels 30:5862–5869